Proceedings of the 6th International and 43rd National Conference on Fluid Mechanics and Fluid Power
December 15-17, 2016, MNNITA, Allahabad, U.P., India

FMFP2016 – Paper No. IN-8

Slot Jet Impingement Heat Transfer using RANS Approach and LES

Anupam Dewan
Department of Applied Mechanics
Indian Institute of Technology Delhi
Hauz Khas, New Delhi - 110016
Email: adewan@am.iitd.ac.in

Rabijit Dutta
Department of Applied Mechanics
Indian Institute of Technology Delhi
Hauz Khas, New Delhi – 110016
Email: rabijit13@gmail.com

Anuj Kumar Shukla
Department of Applied Mechanics
Indian Institute of Technology Delhi
Hauz Khas, New Delhi - 110016
Email: anujshukla.cest@gmail.com

Abstract
Jet impingement heat transfer is an interesting flow configuration to study because of its industrial as well as fundamental importance. Computations of turbulent slot jet impinging flow at a Reynolds number of 20000 and at two values of the nozzle to plate spacing (*H/B*) (where *H* is the channel height and *B* the slot width) equal to 4 and 9.2 have been performed. Various Reynolds-averaged Navier–Stokes (RANS) equations based turbulence models were tested. For a small nozzle to plate spacing of 4 both the standard and SST *k-ω* models showed best agreement with the experimental data. In the case of high nozzle to plate spacing (9.2), some of the models considered showed a false secondary peak in the surface *Nu* and the standard *k-ε* model showed good agreement with the experimental data. Further fluid flow and heat transfer characteristics of slot jet impingement heat transfer at nozzle-to-plate spacing of 4 and 10 with *Re* = 20000 and 13500 were investigated using LES. A secondary peak in *Nu* was observed and reason behind this behaviour is discussed for low nozzle to plate spacing. Large scale vortical structures were observed near the location of the secondary peak in *Nu*.

Keywords: Slot Jet impingement; Heat Transfer; Turbulence Modelling; Nusselt Number.

I. INTRODUCTION

Jet impingement heat transfer is a widely studied flow configuration. It has the maximum heat transfer rate among all the single-phase heat transfer arrangements, and this has led to its increasing use in the industry for cooling, heating, and drying of surfaces. Some typical industrial applications of jet impingement include cooling of electronic equipment, cooling of turbine blades, drying of paper, gas quenching of steel rings, and freezing or drying of various food items. The flow with jet impingement orthogonally on a flat surface follows some distinct regions. At the nozzle exit, the emerging jet may pass through some regions that can be sub-divided into three regions, namely, the potential core, developing and developed regions. At the point where the jet impinges over a flat surface is often referred to as the deflection zone/stagnation region. In this zone, the axial velocity rapidly diminishes with a consequent rise in the static pressure. Thereafter the wall jet region, where the bulk flow is in the radial outward direction, becomes important. The length of the potential core is found to be nearly 4.7 - 7.7 slot widths from the nozzle exit for slot jets [1]. A free jet region may not be present if the nozzle exit lies at a distance of two diameters or slot width from the target plate [2]. Jet impingement heat transfer configuration has been widely studied experimentally by many researchers. Due to its flow complexity it may be considered as a benchmark test for computational models. Recently, Dutta *et al*. [3] reported that the accuracy of predictions by RANS turbulence models depends on the nozzle-to-plate spacing. Those models which predict the secondary peak accurately do not perform well for higher values of the nozzle-to-plate spacing.

Flow and heat transfer behaviours of jet impingement over a flat surface have been widely considered and a large number of experimental and numerical studies have been reported in the literature. Jambunathan *et al.* [4] reviewed a variety of papers dealing with experimental studies on jet impinging flows. Zuckerman and Lior [5] reviewed literature on the accuracy of various RANS based models in predicting jet impinging flow. Recently, Dewan *et al.* [6] presented a comprehensive review of large eddy simulation (LES) studies on jet impingement flows. With a larger value of the nozzle-to-plate spacing (H/B > 6), a peak value of the Nusselt number at the stagnation point can be observed, however, it drops monotonically along the streamwise direction. On the other side, for a low nozzle to plate spacing (H/B < 6) it shows a secondary peak in the local Nusselt number distribution in the streamwise direction. The position of the secondary peak is slightly away from the stagnation point. A number of studies can be found in the literature dealing with the physical reason behind the secondary peak in Nusselt number [7], [8]. Several parameters influence the flow feature and heat transfer characteristics of such flow configurations, such as, flow confinement, nozzle shape, jet to plate spacing, *Re*, etc. The effect of these parameters on the characteristics of slot jet has found special attention in the literature either experimentally or numerically [2], [9], [10], [11] and [12]. Many authors have

suggested that occurrence of the secondary peak could be due to the transition from laminar to turbulent flow in wall jet region.

Majority of the RANS based turbulence models considered in the literature were not able to predict impinging flows accurately and its complexities except a few [3], [13]. Many authors, such as, Cziesla *et al.* [14], Uddin *et al.* [15], Dairay *et al.* [16] and Dutta *et al.* [17], [18] observed that LES is capable of predicting the flow field and heat transfer data within the accepted accuracy limits. But the use of LES is computationally expensive. DNS can be applied to simple geometry with low *Re* [19] and [20]. Development of wall functions for computations is also important for impinging flows [6]. Hadziabdic and Hanjalic [8] performed LES to study round jet impingement heat transfer and reported that the recirculation bubble formed at the wall due to the interaction of the wall jet with the primary vortex. They suggested that the secondary peak could be associated with the reattachment of the recirculation bubble and the associated increase in the turbulence kinetic energy. Recently, Uddin *et al.* [15] also investigated the secondary peak using LES for a round impinging jet heat transfer and associated it with the acceleration of the flow.

Although, few LES studies on jet impinging flow have been reported in the literature lately, most studies have focused on round jet impingement heat transfer [8] and [15]. Further, among various LES studies on slot jet impingement, none have focussed on the secondary peak formation in Nusselt number. Tsubokura *et al.* [21] performed LES for both round and slot jet impingements and compared their eddy structures. Dutta *et al.* [17], [18] performed LES of a slot jet impingement for an identical configuration as that of Beaubert and Viazzo [22] and studied fluid flow and heat transfer rates.

II. METHODOLOGY

In the present study, the computations were performed using an unstructured, cell-centered, finite volume commercial solver ANSYS FLUENT 15 which employs a co-located grid arrangement for solving the governing equations of LES and RANS. The governing equations were solved in their integral forms and interpolations were introduced for the fluxes in the surface integrals. For the discretization of the convective term, a bounded central-difference scheme was used and a second-order central difference scheme was used for the diffusive terms. For the pressure velocity coupling, the semi-implicit pressure linked equations (SIMPLE) method was used. Fig. 1 shows the geometry, grid distribution and boundary conditions used for the present RANS computations. The grids were generated using hexahedral elements for the LES computations (three-dimensional) and rectangular elements for two-dimensional RANS computations. At the inlet, the turbulence quantities, such as, turbulence kinetic energy (k), dissipation rate (ε), and specific dissipation rate (ω) were specified based on a particular turbulence model used. These values were calculated based on the assumption of the fully developed conditions at the nozzle exit. Nozzle exit velocity V_0 based on Reynolds number (Re), I the inlet turbulent intensity ($\frac{v'}{V_0}$) and l the turbulent length scale were specified for the computations.

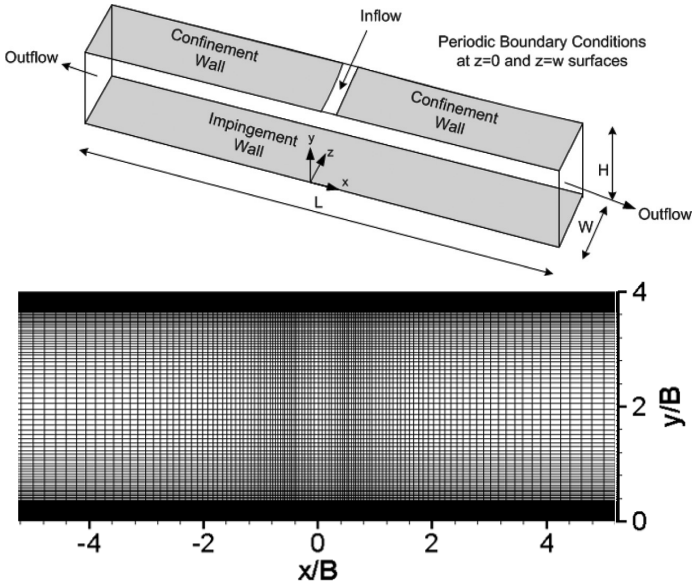


Fig. 1 Computational domain and grid distribution.

For a statistically steady flow, every variable can be written as the sum of average and fluctuating values. In the RANS approach, the time-averaged governing equations were solved. For LES, unsteady, filtered governing equations were solved and the effect of small scales were considered using suitable subgrid scale (SGS) models. In LES, a filtering operation is performed over the equations to separate the motion of the small scales from the large ones. The governing equations for the conservations of mass, momentum and energy for a steady, incompressible flow without body forces can be written as (time-averaged for RANS and filtered for LES)

$$\frac{\partial\left(\rho\overline{U_i}\right)}{\partial x_i}=0 \tag{1}$$

$$\frac{\partial}{\partial x_j}\left(\rho\overline{U}_i\overline{U}_j\right)=-\frac{\partial\overline{P}}{\partial x_i}+\frac{\partial}{\partial x_j}\left[\mu\left(\frac{\partial\overline{U}_i}{\partial x_j}+\frac{\partial\overline{U}_j}{\partial x_i}\right)-\rho\overline{u_i'u_j'}\right] \tag{2}$$

$$\rho c_p\overline{U_i}\frac{\partial\overline{T}}{\partial x_i}=k_a\frac{\partial^2\overline{T}}{\partial x_i^2}-\frac{\partial}{\partial x_i}\left(\rho c_p\overline{u_i'T'}\right) \tag{3}$$

where $\tau_{ij}=\overline{u_iu_j}-\overline{U}_i\overline{U}_j$ is the Reynolds stress for the RANS approach and SGS stress or kinetic Reynolds stress tensor in case of LES. Here ρ denotes fluid density, $\overline{U}_i$ the mean component of velocity in x_i direction and u' the fluctuating component of velocity. The other symbols used here have their standard meanings. Readers are referred to any comprehensive book for

details on turbulence models and detailed formulation of LES used in the present work, such as, Dewan [23].

III. RESULTS AND DISCUSSION

In this section RANS computations of turbulent jet impinging flow at *Re* = 20000, and at two values of nozzle to plate spacing equal to 4 and 9.2 have been performed. All variants of *k-ε* turbulence model, standard *k-ω* and SST *k-ω* have been considered in this study. The predictions were compared with the reported experimental data. The results showed that the accuracy of turbulence models is highly sensitive to the flow conditions. For a small nozzle to plate spacing (4), in which a secondary maxima of Nusselt number is distinct, both the standard and SST *k-ω* models, along with a transitional model, showed the best agreement with the experimental data. In the case of high nozzle to plate spacing (9.2), some of the models considered showed a false secondary peak in the flow. The standard *k-ω* and *k-ε* models only showed good agreement with the experimental data in terms of surface Nusselt number. Here, we tested various values of intensity *I* to fit our computational results with the reported experimental data and observed that at *I* of 1% the computed data showed the best agreement with experimental data [2] in terms of the surface Nusselt number. The turbulence length scale *l* was specified similar to work of Jaramillo *et al.* [20] with *l = 0.015B*.

Fig. 2 shows the surface Nusselt number predictions with various *k-ω* based models. As mentioned earlier, the Nusselt number distribution shows a secondary peak at a lower value of the nozzle-to-plate spacing. The peak in Nusselt number at the stagnation point can be attributed to high velocity associated with the jet impact and the corresponding temperature gradient at the wall. Further, as the flow develops in the wall jet region, the thermal boundary-layer develops and the Nusselt number decreases along the surface. However, the Nusselt number starts increasing and shows a secondary peak, which could be associated with either laminar to turbulent transition or higher turbulence associated with the interaction of the shear layer primary vortices and the secondary vortices at the wall. It can be observed that both the standard *k-ω* and the SST *k-ω* models predict the secondary peak in the Nusselt number when transitional flow model was used. As mentioned earlier, Hofmann *et al.* [24] also observed a similar behavior with better prediction of the secondary peak using the transitional flow model.

Fig. 3 shows the Nusselt number profiles predicted with various *k-ε* models used along with two-layer wall models for *H/B* = 4. The standard *k-ε* model highly overpredicts the value of Nusselt number at the stagnation point. The other two models are able to predict the stagnation point heat transfer; however, both of them did not predict the secondary peak in the Nusselt number.

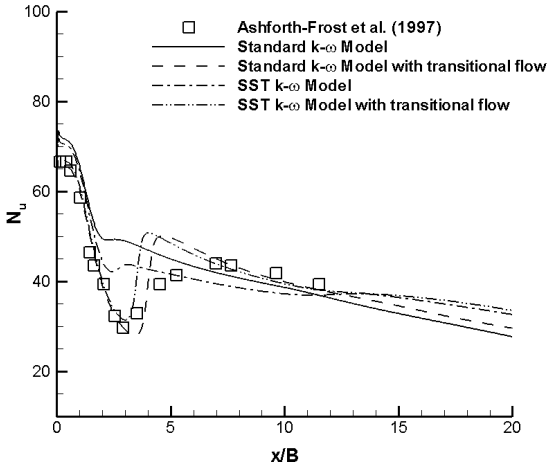


Fig. 2 Surface Nusselt number using various k-ω models for H/B = 4.

For the case of H/B = 9.2, *Nu* distributions using different turbulence models have been plotted in Fig. 4. In contrast to the low nozzle-to-plate spacing case (*H/B* = 4), *Nu* shows a monotonic decrease along the plate. At higher nozzle-to-plate spacings, the jet which impacts the plate carries fully developed turbulence, and therefore, there is no possibility of flow transition. Further, primary vortices break down and lose their strength to have any significant impact on the secondary vortices at the wall. The absence of secondary vortices therefore results in no secondary peak at the wall. It can be observed that all the models predict the stagnation *Nu*; however, except for the standard *k-ω* model, all the other models predict a false secondary peak (Fig. 4). This false secondary peak could be attributed to the poor prediction of entrainment in the free jet region, and consequently, the underprediction of turbulent kinetic energy in the impingement region.

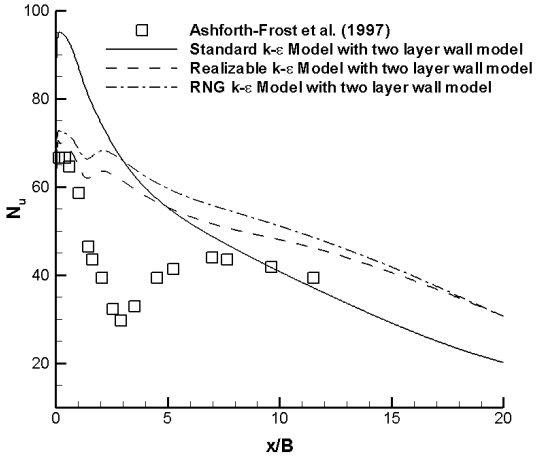


Fig. 3 Surface Nusselt number using various *k-ε* models for *H/B = 4.*

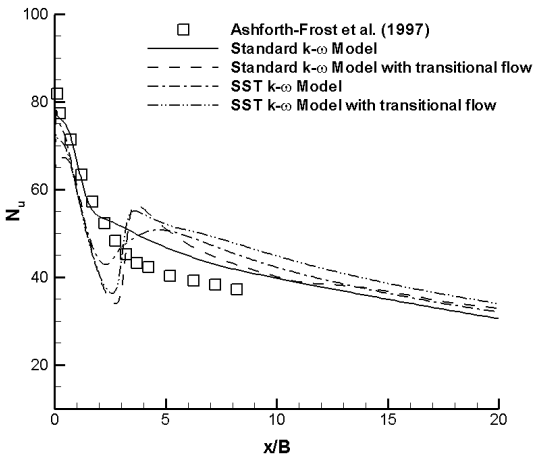


Fig. 4 Surface Nusselt number using various *k-ω* models for *H/B* = 9.2.

The Nusselt number predictions using various *k-ε* models along with two-layer wall models are presented in Fig. 5. It can be observed that the standard *k-ε* model slightly overpredicts the stagnation *Nu*. However, among the three *k-ε* models, the standard *k-ε* model shows the best agreement with the experimental data.

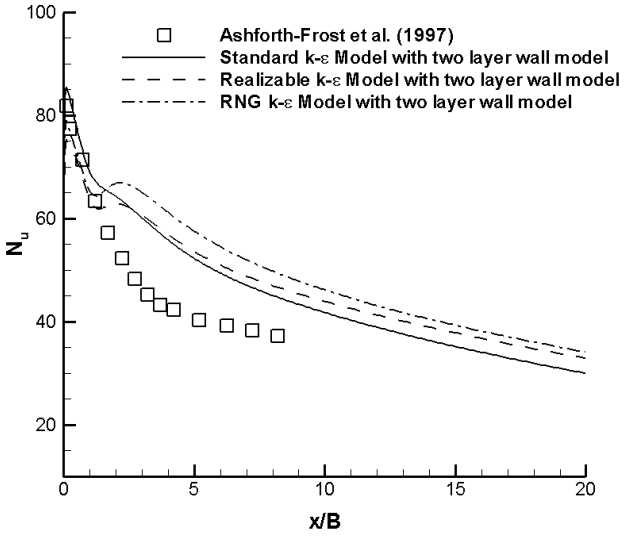
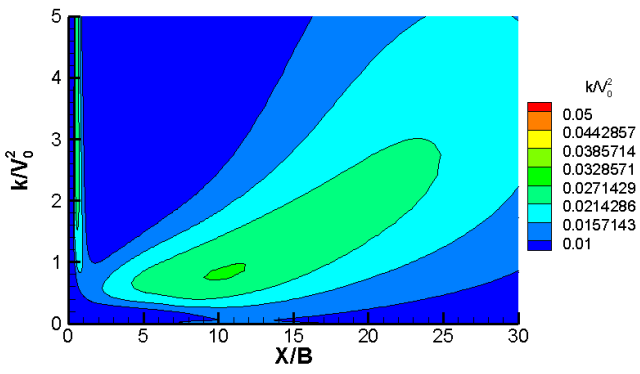


Fig. 5 Surface Nusselt number using various *k-ε* models for H/B = 9.2.



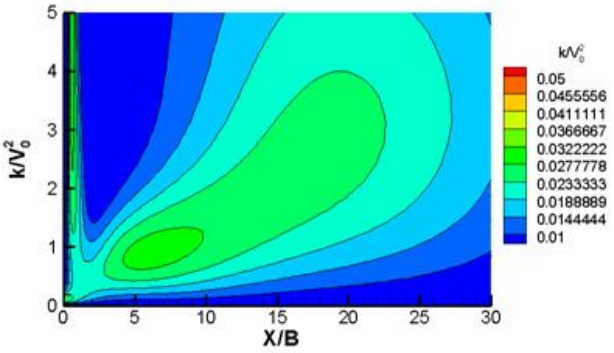


Fig. 6 Comparison of turbulence kinetic energy near the impingement point for *H/B* = 9.2 (a) SST *k-ω* model and (b) standard *k-ε* model with enhanced wall treatment.

Fig. 6 presents the contours of turbulence kinetic energy near the impingement region using SST *k-ω* model (with transitional model) and the standard *k-ε* model to assess if a false secondary peak in *Nu* can be associated with the lower levels of turbulence kinetic energy. It is indeed observed that the SST *k-ω* model contain low levels of turbulence kinetic energy close to the stagnation point, and it increases in the wall jet region which could be the reason for observing a false peak in the Nusselt number distribution. In contrast to these models, the standard *k-ε* model has higher levels of turbulence kinetic energy at the stagnation point; further, it did not show any secondary peak.

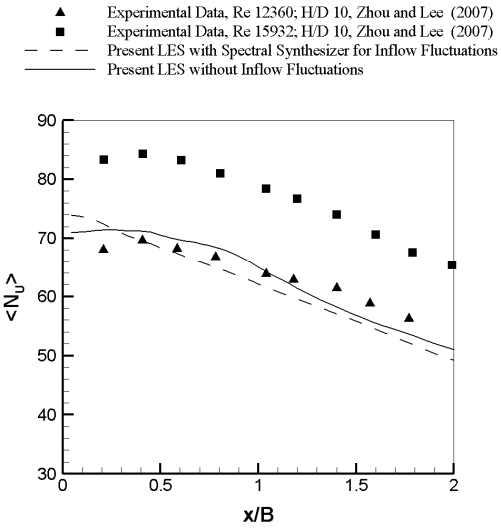


Fig. 7 Nusselt number distributions along the impingement wall.

Now we present LES results for a turbulent slot jet impingement heat transfer at *Re* = 13500 and nozzle to plate spacing of 10. Two inflow conditions, one without any fluctuations and the other with fluctuations generated by the spectral synthesizer were tested, and comparisons of various mean flow, turbulence and heat transfer data showed that LES without any inflow fluctuations provides good agreement with the corresponding experimental and numerical results reported in

the literature. Further, various important dynamical flow structures have been visualized from the instantaneous computed data. The results of Nusselt number distribution along the impingement wall (Fig. 7) are in good agreement with the experimental results of Zhou and Lee [25].

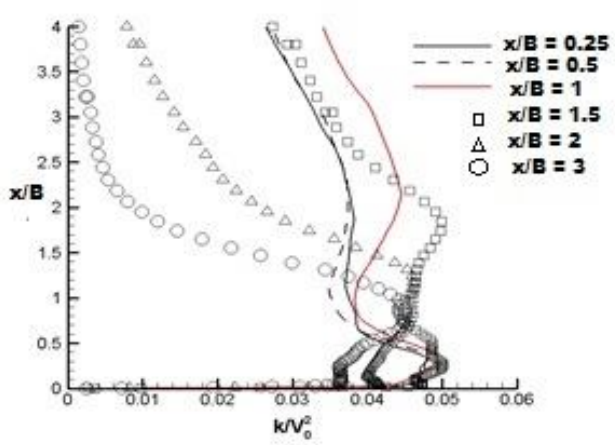


Fig. 8 Turbulence kinetic energy distribution in the wall jet region.

Fig. 8 shows the distribution of turbulence kinetic energy at various streamwise locations in the wall jet region. The maximum kinetic energy (dimensionless) is of the order of 0.04 and this value was also obtained by Cooper *et al.* [26] for round impinging jets. Further, it can be noticed that the peak in kinetic energy is found at x/B = 0.5, which corresponds to the location of the maximum Nusselt number at the impingement wall (Fig. 7). It can be observed from Fig. 9 that the present LES computations have a good resolution of smaller scales of turbulence.

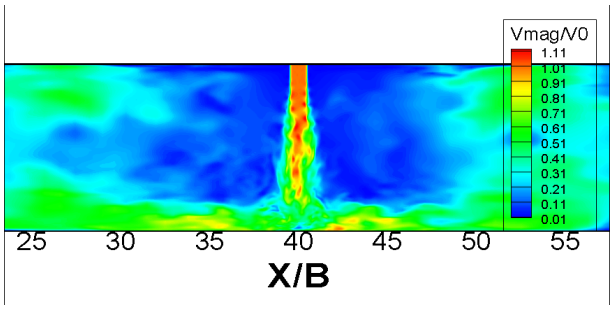


Fig. 9 Instantaneous velocity vectors using LES.

Fluid flow and heat transfer characteristics have been studied in detail using LES for a slot jet impingement heat transfer for a small value of the nozzle-to-plate spacing at which secondary peak in the Nusselt number is observed. Results show that the mean velocity profile in the stagnation region deviates from the standard law of the wall. Further, large scale vortical structures were observed near the location of the secondary *Nu* peak. It was observed that an increase in both the streamwise and wall normal turbulence fluctuations is responsible for the secondary peak in *Nu*. The width of the computational domain in the spanwise direction was taken as 5*B*. This value was found to be appropriate for the application of the periodic conditions based on the computations with different spanwise domain sizes. Further, domain size in the streamwise direction was taken as 80*B*, which was sufficient for the application of the zero-gradient boundary condition. A uniform velocity boundary condition was specified at the exit of the nozzle to match the experimental conditions. Two different turbulence specification techniques, namely, vortex method and no perturbations were used to specify the turbulence at the inlet. Further, temperature at the inlet was set to the ambient value of 300 K. The no-slip conditions were specified for the impingement and confinement walls. A constant temperature of 310 K was set at the impingement wall and a zero heat flux condition was specified at the confinement walls.

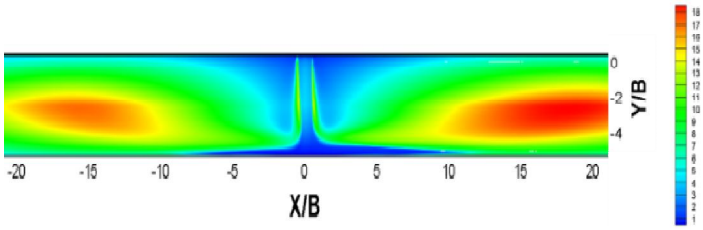


Fig. 10 Ratio of grid size to the Kolmogorov length scale.

Further, the final grid was assessed using the criteria given by Pope [27] and Celik *et al.* [28]. Fig. 10 shows the contours of the ratio of grid size to the Kolmogorov length scale in a plane placed at the centre of the spanwise domain from a RANS computations on the same grid as that used for LES computations. The Kolmogorov length scale (η), defined as $(\nu^3/\varepsilon)^{1/4}$, was calculated using a v^2-f turbulence model on the same grid. It is observed that the region of our interest, $-10 < x/B < 10$, falls within the acceptable range [27]. Moreover, the value of $LESIQ_v$ [28] for the present grid falls in the range of 0.8 – 0.9.

Fig. 11 presents a comparison of the predicted Nusselt number at the impingement wall with the two inflow conditions. We can observe that the vortex method predicts the secondary peak better than the case with no perturbations. In contrast, for LES computations at the large H/B ratio, we observed that the inflow with no perturbations showed better predictions as compared to the spectral synthesizer method for H/B = 10 and Re = 13500. The present behaviour could be attributed to the smaller length of the nozzle-to-plate spacing. As the length is small, the turbulence cannot develop naturally with no inflow perturbations case. This is evident from Fig. 11, where the Nusselt number at the stagnation region was better predicted by the vortex method. The maximum Nusselt number is slightly off from the axis, because of the higher turbulence levels at the jet shear layer. Further, as shown in Fig. 11, LES with the vortex method showed a better prediction of the secondary peak as compared to the case with no perturbations.

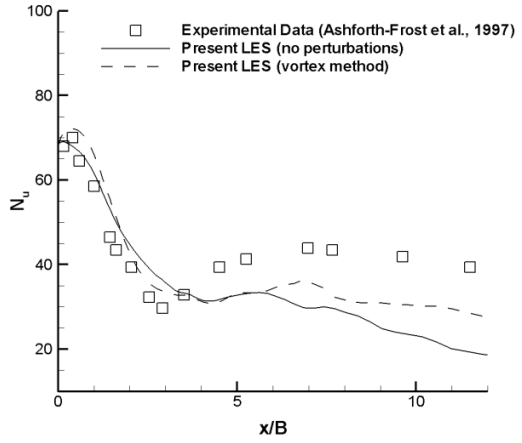


Fig. 11 Comparison of surface Nusselt number for two inflow conditions

IV. CONCLUSIONS

Computations of turbulent slot jet impinging flow have been performed in the present study. Various Reynolds-averaged Navier–Stokes (RANS) equations based turbulence models were tested. For a small nozzle to plate spacing of 4 both the standard and SST k-ω models showed the best agreement with the experimental data. In the case of high nozzle to plate spacing (9.2), some of the models considered showed a false secondary peak in the surface Nusselt number and the standard k-ε model showed good agreement with the experimental data. Further fluid flow and heat transfer characteristics of slot jet impingement heat transfer at nozzle-to-plate spacing of 4 and 10 with Re = 20000 and 13500 were investigated using LES. A secondary peak in the Nusselt number was observed and reason behind this is discussed for low nozzle to plate spacing. Large scale vortical structures were observed near the location of the secondary peak in Nusselt number. Two inflow conditions, one without any fluctuations and the other with fluctuations, generated by the spectral synthesizer, were tested and comparisons of various data showed that LES without any inflow fluctuations provided good agreement with the corresponding experimental and numerical results reported in the literature.

REFERENCES

1. J.N.B. Livingood, P. Hrycak, Impingement heat transfer from turbulent air jets to flat plates: A literature survey, *Security.* X-2778 (1973) 43.

2. S. Ashforth-Frost, K. Jambunathan, C.F. Whitney, Velocity and turbulence characteristics of a semiconfined orthogonally impinging slot jet, *Exp. Therm. Fluid Sci. 14* (1997) 60–67.

3. R. Dutta, A. Dewan, B. Srinivasan, Comparison of various integration to wall (ITW) RANS models for predicting turbulent slot jet impingement heat transfer, *Int. J. Heat Mass Transf. 65* (2013) 750–764.

4. K. Jambunathan, E. Lai, M. A. Moss, B.L. Button, A review of heat transfer data for single circular jet impingement, *Exp. Therm. Fluid Sci. 33* (2005) 106–115.

5. N. Zuckerman, N. Lior, Jet impingement heat transfer: Physics, correlations, and numerical modeling, *Adv. Heat Transf. 39* (2006) 565–631.

6. A. Dewan, R. Dutta, B. Srinivasan, Recent trends in computation of turbulent jet impingement heat transfer, *Heat Transf. Eng. 33* (2012) 447–460.

7. R. Gardon, J.C. Akfirat, The role of turbulence in determining the heat-transfer characteristics of impinging jets, *Int. J. Heat Mass Transf. 8* (1965) 1261–1272.

8. M. Hadžiabdić, K. Hanjalić, Vortical structures and heat transfer in a round impinging jet, *J. Fluid Mech. 596* (2008) 221–260.

9. S. Ashforth-Frost, K. Jambunathan, Effect of nozzle geometry and semi-confinement on the potential core of a turbulent axisymmetric free jet, *Int. Commun. Heat Mass Transf. 23* (1996) 155–162.

10. C.J. Hoogendoorn, The effect of turbulence on heat transfer at a stagnation point, *Int. J. Heat Mass Transf. 20* (1977) 1333–1338.

11. J. Zhe, V. Modi, Near Wall Measurements for a Turbulent Impinging Slot Jet, *J. Fluids Eng. 123* (2001) 112–120.

12. D. Lytle, B.W. Webb, Air jet impingement heat transfer at low nozzle-plate spacings, *Int. J. Heat Mass Transf. 31* (1994) 1687–1697.

13. M. Behnia, S. Parneix, Y. Shabany, P. a. Durbin, Numerical study of turbulent heat transfer in confined and unconfined impinging jets, *Int. J. Heat Fluid Flow 20* (1999) 1–9.

14 T. Cziesla, G. Biswas, H. Chattopadhyay, N.K.K. Mitra, Large-eddy simulation of flow and heat transfer in an impinging slot jet, *Int. J. Heat Fluid Flow 22* (2001) 500–508.

15. N. Uddin, S.O. Neumann, B. Weigand, LES simulations of an impinging jet: On the origin of the second peak in the Nusselt number distribution, *Int. J. Heat Mass Transf. 57* (2013) 356–368.

16. T. Dairay, V. Fortuné, E. Lamballais, L.E. Brizzi, LES of a turbulent jet impinging on a heated wall using high-order numerical schemes, *Int. J. Heat Fluid Flow 50* (2014) 177–187.

17. R. Dutta, A. Dewan, B. Srinivasan, Large Eddy Simulation of Turbulent Slot Jet Impingement Heat Transfer at Small Nozzle-to-Plate Spacing, *Heat Transf. Eng. 37* (2016) 12242-1251.

18. R. Dutta, B. Srinivasan, A. Dewan, LES of a turbulent slot impinging jet to predict fluid flow and heat transfer, *Numer. Heat Transf. Part A Appl. 64* (2013) 759–776.

19. Y.M.M. Chung, K.H.H. Luo, N.D.D. Sandham, Numerical study of momentum and heat transfer in unsteady impinging jets, *Int. J. Heat Fluid Flow 23 (2002)* 592–600.

20. J.E. Jaramillo, F.X. Trias, A. Gorobets, C.D. Pérez-Segarra, A. Oliva, DNS and RANS modelling of a turbulent plane impinging jet, *Int. J. Heat Mass Transf. 55* (2012) 789–801.

21. M. Tsubokura, T. Kobayashi, N. Taniguchi, W.P. Jones, A numerical study on the eddy structures of impinging jets excited at the inlet, *Int. J. Heat Fluid Flow 24* (2003) 500–511.

22. F. Beaubert, S. Viazzo, Large eddy simulations of plane turbulent impinging jets at moderate Reynolds numbers, *Int. J. Heat Fluid Flow 24* (2003) 512–519.

23. A. Dewan, Tackling Turbulent Flows in Engineering, *Springer* Berlin Heidelberg, Berlin, Heidelberg, 2011.

24. H.M. Hofmann, R. Kaiser, M. Kind, H. Martin, Calculations of Steady and Pulsating Impinging Jets—An Assessment of 13 Widely used Turbulence Models, *Numer. Heat Transf. Part B Fundam. 51* (2007) 565–583.

25. D.W. Zhou, S.J. Lee, Forced convective heat transfer with impinging rectangular jets, *Int. J. Heat Mass Transf. 50* (2007) 1916–1926.

26. D. Cooper, D.C. Jackson, B.E. Launder, G.X Liao, Impinging Jet Studies for Turbulence Model Assesment - I. Flow Field Experiemnts, *Int. J. Heat Mass Transf.* 36 (1993) 2675–2684.

27. S.B. Pope, Ten Questions Concerning the Large Eddy Simulation of Turbulent Flows, In: Large Eddy Simulation and subgrid-Scale Modeling for Turbulent Mixing and Reactive Flows, in: *Calif. Inst. Technol.* USA, 2003.

28. I. Celik, Z.N. Cehreli, I. Yavuz, Index of Resolution Quality for Large Eddy Simulations, *J. Fluids Eng. 127* (2005) 949-958.